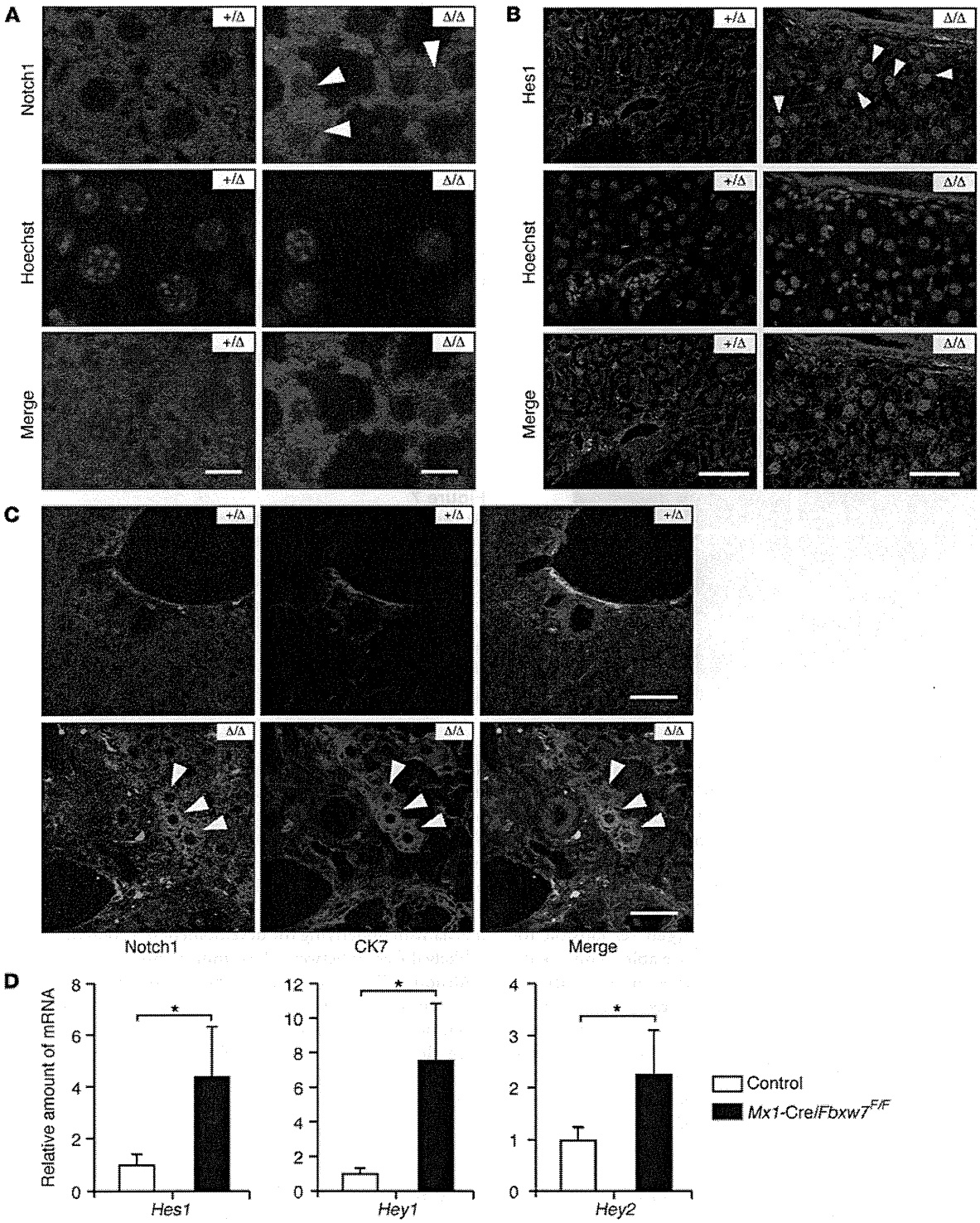

Figure 6

Accumulation of Notch1 and activation of its target genes in the Fbxw7-deficient liver. (**A** and **B**) Representative immunostaining for the intracellular domain of (**A**) Notch1 and for (**B**) Hes1 in liver sections from *Mx1*-Cre/*Fbxw7*$^{+/F}$ (+/Δ) and *Mx1*-Cre/*Fbxw7*$^{F/F}$ (Δ/Δ) mice at 3 weeks after *Fbxw7* deletion by pIpC injection, beginning at 8 weeks of age. Arrowheads indicate accumulating (**A**) Notch1 intracellular domain and (**B**) Hes1 in the nucleus. (**C**) Immunofluorescence staining for the intracellular domain of Notch1 and for CK7 in the livers of *Mx1*-Cre/*Fbxw7*$^{+/F}$ (+/Δ) and *Mx1*-Cre/*Fbxw7*$^{F/F}$ (Δ/Δ) mice at 15 weeks after the final injection of pIpC, beginning at 8 weeks of age. Intense Notch1 staining was detected in the Fbxw7-deficient liver, and most of the Notch1-positive cells express CK7 (arrowheads). Scale bar: 10 μm (**A**); 50 μm (**B** and **C**). (**D**) RT and real-time PCR analysis of Notch target genes in the livers of *Mx1*-Cre/*Fbxw7*$^{+/F}$ (control) and *Mx1*-Cre/*Fbxw7*$^{F/F}$ mice at 50 weeks after *Fbxw7* deletion. Normalized data for *Hes1*, *Hey1*, and *Hey2* mRNAs are expressed relative to the corresponding value for control mice and are mean ± SD from 3 independent experiments. *$P < 0.05$.

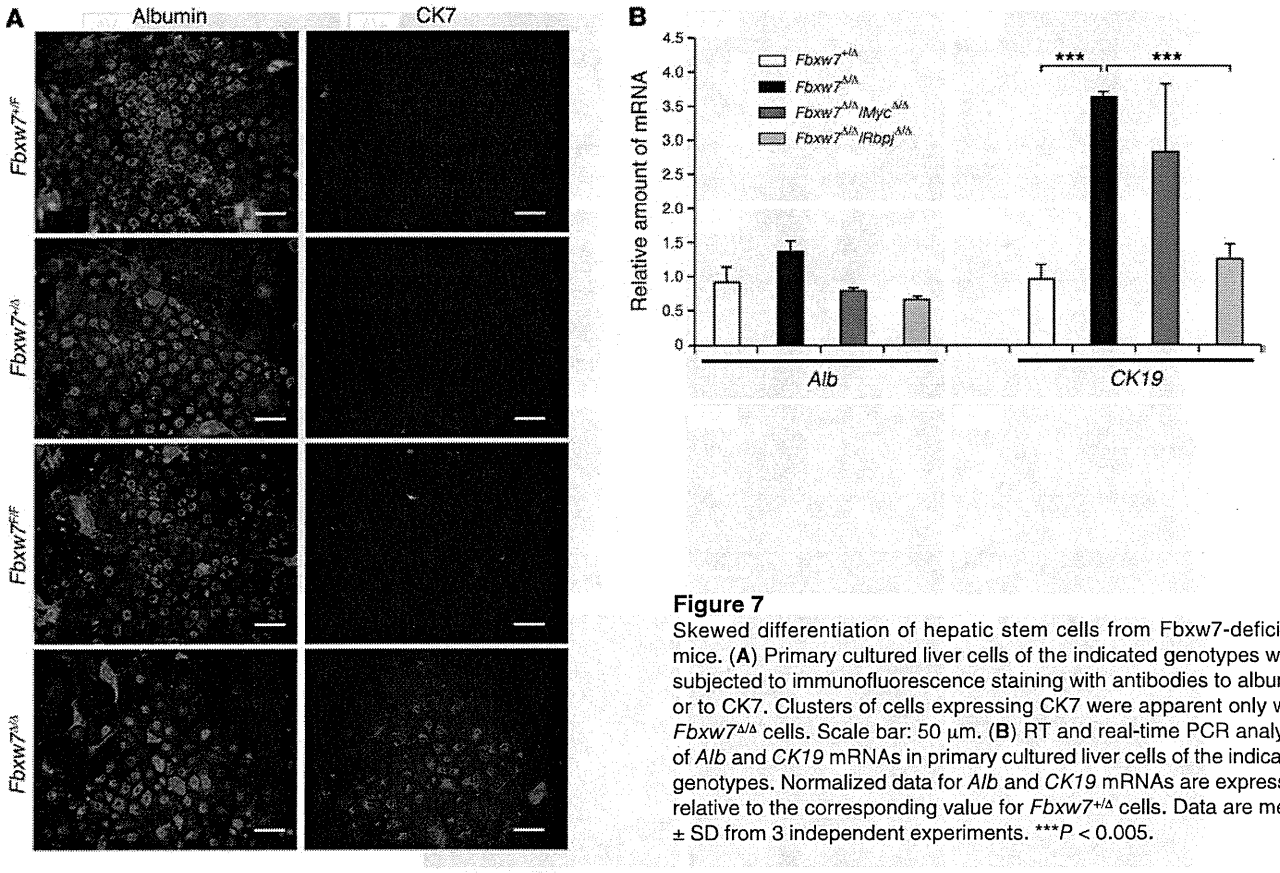

Figure 7

Skewed differentiation of hepatic stem cells from Fbxw7-deficient mice. (**A**) Primary cultured liver cells of the indicated genotypes were subjected to immunofluorescence staining with antibodies to albumin or to CK7. Clusters of cells expressing CK7 were apparent only with *Fbxw7*$^{\Delta/\Delta}$ cells. Scale bar: 50 μm. (**B**) RT and real-time PCR analysis of *Alb* and *CK19* mRNAs in primary cultured liver cells of the indicated genotypes. Normalized data for *Alb* and *CK19* mRNAs are expressed relative to the corresponding value for *Fbxw7*$^{+/\Delta}$ cells. Data are mean ± SD from 3 independent experiments. ***$P < 0.005$.

activation and development of hamartoma in humans (54, 55). However, the abundance of mTOR or TSC1/2 was not altered in the Fbxw7-deficient livers of mice, suggesting that the accumulation of mTOR or the loss of TSC1/2 is not responsible for hamartoma development in these animals. Microscopic examination revealed over proliferation of the biliary system in the hamartomas, suggesting that deregulated differentiation of liver stem cells into the cholangiocyte lineage might be largely responsible for hamartoma development. Liver stem cells are able to differentiate into either the hepatocyte or cholangiocyte lineages, with the Notch signaling pathway having been implicated in regulation of the cell fate decision by skewing differentiation toward the cholangiocyte lineage (41). We have now shown that both Notch1 and its target genes were overexpressed in the Fbxw7-deficient livers of mice and that the abnormal cell differentiation induced by Fbxw7 loss was corrected by the additional loss of the Notch cofactor RBP-J. These results suggest that Notch1 accumulation as a result of Fbxw7 loss is primarily responsible for the abnormal cell differentiation in the Fbxw7-deficient mouse liver. Although the origin of hamartomas as well as the mechanism of their development in the Fbxw7-deficient liver are currently unclear, transient activation of Notch proteins as a result of Fbxw7 loss may lead to a shift in cell differentiation from hepatocytes to cholangiocytes, and the generation of such abnormally differentiated cells might confer a predisposition to hamartoma development that is realized if the cells undergo an additional gene mutation. Mice lacking both Foxa1 and Foxa2 were recently shown to display a similar liver phenotype (hyperplasia of the biliary tree) (56). However, neither differentiation of hepatocytes nor Notch signaling were affected in Foxa1/2-deficient mice, whereas hyperactivation of Notch signaling seems to be attributable to the bile duct hamartoma in Fbxw7-deficient mice. Furthermore, proliferation of relatively small and uniform bile ducts is prominent in Foxa1/2-deficient mice, whereas the abnormal bile ducts in Fbxw7-deficient mice are large and heterogeneous in size. We therefore concluded that the mechanism underlying the development of proliferative bile ducts is likely different between these mutant mice.

Although Fbxw7 had been thought to function primarily in cell cycle control by regulating cyclin E, c-Myc, Notch, and c-Jun, the recent identification of additional substrates has suggested new cell cycle–independent roles for Fbxw7. We now provide genetic evidence that the major substrates of Fbxw7 in the liver are SREBP1 and Notch1, which accumulate in the Fbxw7-deficient liver and are responsible for liver steatosis and hamartoma development, respectively. These results contrast with our previous observations that deletion of *Fbxw7* in the hematopoietic system and fibroblasts results primarily in deregulation of the cell cycle or of apoptosis due to activation of the p53-dependent checkpoint (34–36). Why does the function of Fbxw7 differ in different tissues? We propose that the biological relevance of Fbxw7 is determined by 3 factors: (a) the expression of Fbxw7; (b) the expression and activation of protein kinases that phosphorylate the Cdc4 phosphodegron, an amino acid sequence that is recognized by Fbxw7; and (c) the expression of substrate molecules. The combination of these 3 factors may define the role of Fbxw7 in a tissue-specific manner, with the different phenotypes associated with Fbxw7 deficiency

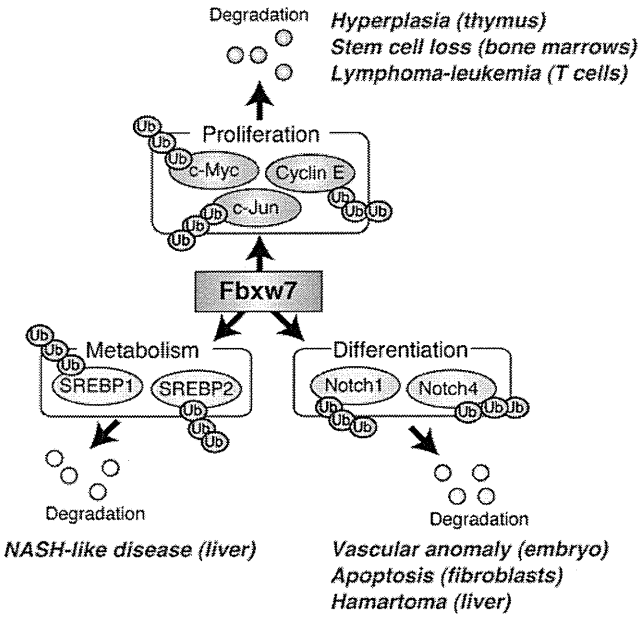

Figure 8
A model for Fbxw7 functions in vivo. Fbxw7 mediates ubiquitin-dependent degradation of substrates in different functional categories. For example, Fbxw7 controls cell proliferation by targeting c-Myc, cyclin E, and c-Jun for degradation. However, it also regulates lipid metabolism and cell differentiation by targeting SREBP and Notch proteins, respectively. Major phenotypes associated with Fbxw7 deficiency in different tissues are shown in red. Ub, ubiquitin.

being attributable to different expression patterns of Fbxw7, its substrates, and kinases that phosphorylate each substrate.

Methods

Generation of conditional knockout mice. Mice homozygous for the floxed *Fbxw7* allele (*Fbxw7*$^{F/F}$ mice) (34) were crossed with *Mx1*-Cre transgenic mice (57) provided by K. Rajewsky (Harvard Medical School, Boston, Massachusetts, USA) or *Alb*-Cre transgenic mice (58) purchased from The Jackson Laboratory. Expression of Cre recombinase in the resulting offspring of the former cross was induced by i.p. injection of 500 μg pIpC (GE Healthcare Biosciences) on 3 alternate days. Deletion of exon 5 of the floxed *Fbxw7* allele was confirmed by PCR analysis of genomic DNA as previously described (34). *Fbxw7*$^{F/F}$ mice were also crossed with *Rbpj*$^{F/F}$ mice (59) provided by T. Honjo (Kyoto University, Kyoto, Japan) or *Myc*$^{F/F}$ mice (60) provided by I.M. de Alborán (National Center for Biotechnology, Madrid, Spain). The experimental protocols were approved by the Institutional Animal Care and Use Committee of Kyushu University.

Histological and biochemical analysis. Liver tissue was fixed with 4% paraformaldehyde in PBS, embedded in paraffin, and stained with H&E or Masson's trichrome solution. Some sections were stained with Oil red O (Nakalai Tesque) according to standard procedures, in order to examine the extent of lipid accumulation in hepatocytes. Serum levels of AST and ALT were measured with a standard clinical autoanalyzer.

Dietary model of NASH. Mice were fed with an MCD diet (Funabashi Farm) for the indicated periods (see the legend for Figure 2) and analyzed.

Measurement of triglyceride and total cholesterol levels in the liver. Frozen liver tissue was homogenized, and triglyceride and total cholesterol were extracted from the homogenate with chloroform/methanol (2:1, vol/vol), dried, and resuspended in 2-propanol. The amounts of triglyceride and total cholesterol in the extract were measured with the use of Lipidos liquid and Cholescolor liquid kits (Toyobo), respectively.

Immunoblot analysis. Total protein extracts were prepared from liver with RIPA buffer. The extracts (30 μg) were subjected to immunoblot analysis as described previously (61) with antibodies to cyclin E (M-20), to c-Myc (N-262), to ChREBP (P-13), or to PPAR-γ (E-8), all of which were obtained from Santa Cruz Biotechnology Inc.; with antibodies to Ser^{2448}-phosphorylated or total (7C10) forms of mTOR (Cell Signaling Technology); with antibodies to SREBP1 (2A4, NeoMarkers); or with antibodies to PGC-1α (Chemicon). As a control, each membrane was stripped and then probed with antibodies to Hsp90 (BD Transduction Laboratories).

RT and real-time PCR analysis. Total RNA was extracted from liver using the guanidinium thiocyanate–phenol-chloroform method, purified, and subjected (1 μg) to RT with random hexanucleotide primers (ReverTra Ace α, Toyobo). The resulting cDNA was subjected to real-time PCR in a reaction mixture that contained 1× SYBR Green PCR Master Mix (Applied Biosystems) and 200 nM of gene-specific primers. Assays were performed in triplicate with an ABI Prism 7700 Sequence Detector (Applied Biosystems). The PCR protocol comprised 40 cycles of incubation at 60°C for 30 seconds and 95°C for 5 seconds. The sequences of the PCR primers (sense and antisense, respectively) were 5′-TGCTCCCAGCTGCAGGC-3′ and 5′-GCCCGGTAGCTCTGGGTGTA-3′ for *Fas*, 5′-TGGGTTGGCTGCTTGTG-3′ and 5′-GCGTGGGCAGGATGAAG-3′ for *Scd1*, 5′-CTGCCGACCTGATGAATTCC-3′ and 5′-TAGGGCCATCACACTGTGTC-3′ for *Ldlr*, 5′-GCTCTCCATACAGTGCTACC-3′ and 5′-GAGTGAAAGATCATGAAGCC-3′ for *Hmgcs1*, 5′-AGAGATGCCATCTCCAGCCTC-3′ and 5′-CTTGGTCTTAGGGTCTTCAGG-3′ for *ChREBP*, 5′-CTGTGAAGTTCAATGCACTGGAA-3′ and 5′-CCTCGATGGGCTTCACGTT-3′ for *Pparg*, 5′-CATGGATTGCACATTTGAAG-3′ and 5′-CCTGTGTCCCCTGTCTCA-3′ for *SREBP1c*, 5′-TCCTGTGCTGCAGCCTTTCTCA-3′ and 5′-CCAGGTTCCCACAAAGGCATCA-3′ for fatty acid–binding protein 4, 5′-GTCCTACAGATTGACAATGC-3′ and 5′-CACGCTCTGGATCTGTGACAG-3′ for *CK19*, 5′-CATGACACCATGCCTGCTGAT-3′ and 5′-CTCTGATCTTCAGGAAGTGTAC-3′ for *Alb*, 5′-CATTCCAAGCTAGAGAAGGCAG-3′ and 5′-TATTTCCCCAACACGCTCG-3′ for *Hes1*, 5′-AAAATGCTGCACACTGCAGG-3′ and 5′-CGAGTCCTTCAATGATGCTCAG-3′ for *Hey1*, 5′-AAACGACCTCCGAAAGCGA-3′ and 5′-CGGTGAATTGGACCTCATCACT-3′ for *Hey2*, and 5′-GGAACATAGCCGTAAACTGC-3′ and 5′-TCACTGTGCCTGAACTTACC-3′ for β-tubulin. Reactions for β-tubulin mRNA were performed concurrently on the same plate as those for the test mRNAs, and results were normalized by the corresponding amount of β-tubulin mRNA.

BrdU incorporation in vivo. Mice were injected with BrdU (1 mg, i.p.) on 3 consecutive days. The liver was removed 24 hours after the third injection of BrdU, and BrdU incorporation was examined with an In Situ BrdU Detection Kit (BD Biosciences). BrdU-positive cells were counted in 10 different fields at high (×400) magnification, and the percentage of BrdU-positive cells was calculated.

Immunofluorescence microscopy. Liver tissue was fixed with 4% paraformaldehyde in PBS and sectioned at a thickness of 40 μm with a vibratome. Sections were then immunostained with antibodies to the intracellular domain of Notch1 or to SCD-1 (both from Cell Signaling Technology), to Hes1 (AB5702, Millipore), to SREBP1 (2A4, NeoMarkers), to albumin (Biogenesis), to CK19 (45), or to CK7 (MAB3226, Chemicon). Immune complexes were detected with Alexa Fluor 488– or Alexa Fluor 546–conjugated goat antibodies to mouse or rabbit IgG (Invitrogen). Cultured liver cells were also subjected to immunostaining, as described previously (45), with the antibodies to albumin and to CK7. For confocal microscopic analysis, we used Zeiss LSM 510 META Confocal Microscope (Carl Zeiss MicroImaging).

TUNEL assay. The TUNEL assay was performed as described previously (62). In brief, paraffin-embedded sections of liver were treated with H_2O_2,

permeabilized for 15 minutes at 37°C with proteinase K (20 μg/ml, Sigma-Aldrich), and then incubated for 1 hour at 37°C with a reaction mixture containing terminal deoxynucleotidyl transferase (Invitrogen) and biotinylated dUTP (Boehringer Ingelheim). Labeled DNA was visualized with an ABC Kit (Vector Laboratories) and diaminobenzidine.

Primary culture of fetal hepatocytes. For the preparation of a single-cell suspension, the livers of mice at E13.5 were dissociated in culture medium (DMEM supplemented with 10% FBS, γ-insulin [1 μg/ml, Wako], 0.1 μM dexamethasone [Sigma-Aldrich], 10 mM nicotinamide [Sigma-Aldrich], 2 mM L-glutamine [Gibco BRL], 50 μM β-mercaptoethanol [Sigma-Aldrich], 5 mM HEPES [Wako], and penicillin-streptomycin [Gibco BRL]) by repeated passage of the tissue through the mouth of a pipette. Human recombinant HGF (50 ng/ml, Sigma-Aldrich) and EGF (20 ng/ml, Sigma-Aldrich) were added to the cells at 24 hours after culture initiation. Cells were seeded at a density of 1×10^6 cells per well in 6-well plates for infection with retroviruses as described below (45).

Gene deletion in cultured cells by retroviral infection. cDNA encoding Cre recombinase was subcloned into the retroviral vector pMX-puro provided by T. Kitamura (University of Tokyo, Tokyo, Japan), and the resulting construct was introduced into Plat E packaging cells (63) with the use of the FuGENE6 reagent (Roche). The resulting culture supernatants containing the recombinant ecotropic retrovirus were harvested and incubated for 24 hours in the presence of Polybrene (2 μg/ml; Sigma-Aldrich) with proliferating liver cells harboring floxed alleles of *Fbxw7*, *Rbpj*, or *Myc*. The cells were cultured for an additional 24 hours in virus-free medium, subjected to selection in medium containing puromycin (3 μg/ml), cultured for 96 hours in puromycin-free medium, and then harvested.

Statistics. Data are presented as mean ± SD and were analyzed using 2-tailed Student's *t* test. A *P* value of less than 0.05 was considered statistically significant.

Acknowledgments

We thank T. Honjo for *Rbpj* floxed mice; I.M. de Alborán for *Myc* floxed mice; K. Rajewsky for *Mx1*-Cre transgenic mice; T. Kitamura for pMX-puro; S. Aishima, Y. Nishihara, M. Sakamoto, and R. Irie for discussion; N. Kitajima, Y. Yamada, and K. Takeda for technical assistance; members of our laboratories for comments on the manuscript; and A. Ohta and M. Kimura for help in the preparation of the manuscript. This work was supported in part by a grant from the Ministry of Education, Culture, Sports, Science, and Technology of Japan and by a research grant from the Takeda Science Foundation.

Received for publication August 6, 2009, and accepted in revised form September 29, 2010.

Address correspondence to: Keiichi I. Nakayama, Department of Molecular and Cellular Biology, Medical Institute of Bioregulation, Kyushu University, 3-1-1 Maidashi, Higashi-ku, Fukuoka, Fukuoka 812-8582, Japan. Phone: 81.92.642.6815; Fax: 81.92.642.6819; E-mail: nakayak1@bioreg.kyushu-u.ac.jp.

1. Hershko A, Ciechanover A. The ubiquitin system. *Annu Rev Biochem.* 1998;67:425–479.
2. Nakayama KI, Nakayama K. Ubiquitin ligases: cell-cycle control and cancer. *Nat Rev Cancer.* 2006; 6(5):369–381.
3. Frescas D, Pagano M. Deregulated proteolysis by the F-box proteins SKP2 and beta-TrCP: tipping the scales of cancer. *Nat Rev Cancer.* 2008;8(6):438–449.
4. Welcker M, Clurman BE. FBW7 ubiquitin ligase: a tumour suppressor at the crossroads of cell division, groWTh and differentiation. *Nat Rev Cancer.* 2008;8(2):83–93.
5. Hubbard EJ, Wu G, Kitajewski J, Greenwald I. *sel-10*, a negative regulator of *lin-12* activity in *Caenorhabditis elegans*, encodes a member of the CDC4 family of proteins. *Genes Dev.* 1997;11(23):3182–3193.
6. Sundaram M, Greenwald I. Suppressors of a *lin-12* hypomorph define genes that interact with both *lin-12* and *glp-1* in *Caenorhabditis elegans*. *Genetics.* 1993;135(3):765–783.
7. Gupta-Rossi N, et al. Functional interaction between SEL-10, an F-box protein, and the nuclear form of activated Notch1 receptor. *J Biol Chem.* 2001;276(37):34371–34378.
8. Oberg C, Li J, Pauley A, Wolf E, Gurney M, Lendahl U. The Notch intracellular domain is ubiquitinated and negatively regulated by the mammalian Sel-10 homolog. *J Biol Chem.* 2001;276(38):35847–35853.
9. Koepp DM, et al. Phosphorylation-dependent ubiquitination of cyclin E by the SCF^{Fbw7} ubiquitin ligase. *Science.* 2001;294(5540):173–177.
10. Moberg KH, Bell DW, Wahrer DC, Haber DA, Hariharan IK. Archipelago regulates Cyclin E levels in Drosophila and is mutated in human cancer cell lines. *Nature.* 2001;413(6853):311–316.
11. Strohmaier H, Spruck CH, Kaiser P, Won KA, Sangfelt O, Reed SI. Human F-box protein hCdc4 targets cyclin E for proteolysis and is mutated in a breast cancer cell line. *Nature.* 2001;413(6853):316–322.
12. Yada M, et al. Phosphorylation-dependent degradation of c-Myc is mediated by the F-box protein Fbw7. *EMBO J.* 2004;23(10):2116–2125.
13. Welcker M, et al. The Fbw7 tumor suppressor regulates glycogen synthase kinase 3 phosphorylation-dependent c-Myc protein degradation. *Proc Natl Acad Sci U S A.* 2004;101(24):9085–9090.
14. Nateri AS, Riera-Sans L, Da Costa C, Behrens A. The ubiquitin ligase SCF^{Fbw7} antagonizes apoptotic JNK signaling. *Science.* 2004;303(5662):1374–1378.
15. Wei W, Jin J, Schlisio S, Harper JW, Kaelin WG Jr. The v-Jun point mutation allows c-Jun to escape GSK3-dependent recognition and destruction by the Fbw7 ubiquitin ligase. *Cancer Cell.* 2005;8(1):25–33.
16. Sundqvist A, et al. Control of lipid metabolism by phosphorylation-dependent degradation of the SREBP family of transcription factors by SCF^{Fbw7}. *Cell Metab.* 2005;1(6):379–391.
17. Punga T, Bengoechea-Alonso MT, Ericsson J. Phosphorylation and ubiquitination of the transcription factor sterol regulatory element-binding protein-1 in response to DNA binding. *J Biol Chem.* 2006;281(35):25278–25286.
18. Bengoechea-Alonso MT, Ericsson J. A phosphorylation cascade controls the degradation of active SREBP1. *J Biol Chem.* 2009;284(9):5885–5895.
19. Mao JH, et al. FBXW7 targets mTOR for degradation and cooperates with PTEN in tumor suppression. *Science.* 2008;321(5895):1499–1502.
20. Olson BL, et al. SCF^{Cdc4} acts antagonistically to the PGC-1alpha transcriptional coactivator by targeting it for ubiquitin-mediated proteolysis. *Genes Dev.* 2008;22(2):252–264.
21. Maser RS, et al. Chromosomally unstable mouse tumours have genomic alterations similar to diverse human cancers. *Nature.* 2007;447(7147):966–971.
22. Lee JW, et al. Mutational analysis of the hCDC4 gene in gastric carcinomas. *Eur J Cancer.* 2006; 42(14):2369–2373.
23. Kemp Z, et al. CDC4 mutations occur in a subset of colorectal cancers but are not predicted to cause loss of function and are not associated with chromosomal instability. *Cancer Res.* 2005; 65(24):11361–11366.
24. Hubalek MM, et al. Cyclin E dysregulation and chromosomal instability in endometrial cancer. *Oncogene.* 2004;23(23):4187–4192.
25. Koh MS, Ittmann M, Kadmon D, Thompson TC, Leach FS. CDC4 gene expression as potential biomarker for targeted therapy in prostate cancer. *Cancer Biol Ther.* 2006;5(1):78–83.
26. Calhoun ES, et al. BRAF and FBXW7 (CDC4, FBW7, AGO, SEL10) mutations in distinct subsets of pancreatic cancer: potential therapeutic targets. *Am J Pathol.* 2003;163(4):1255–1260.
27. Akhoondi S, et al. FBXW7/hCDC4 is a general tumor suppressor in human cancer. *Cancer Res.* 2007;67(19):9006–9012.
28. Song JH, Schnittke N, Zaat A, Walsh CS, Miller CW. FBXW7 mutation in adult T-cell and B-cell acute lymphocytic leukemias. *Leuk Res.* 2008; 32(11):1751–1755.
29. Thompson BJ, et al. The SCF^{FBW7} ubiquitin ligase complex as a tumor suppressor in T cell leukemia. *J Exp Med.* 2007;204(8):1825–1835.
30. O'Neil J, et al. FBW7 mutations in leukemic cells mediate NOTCH pathway activation and resistance to gamma-secretase inhibitors. *J Exp Med.* 2007;204(8):1813–1824.
31. Malyukova A, et al. The tumor suppressor gene hCDC4 is frequently mutated in human T-cell acute lymphoblastic leukemia with functional consequences for Notch signaling. *Cancer Res.* 2007;67(12):5611–5616.
32. Tsunematsu R, et al. Mouse Fbw7/Sel-10/Cdc4 is required for notch degradation during vascular development. *J Biol Chem.* 2004;279(10):9417–9423.
33. Tetzlaff MT, et al. Defective cardiovascular development and elevated cyclin E and Notch proteins in mice lacking the Fbw7 F-box protein. *Proc Natl Acad Sci U S A.* 2004;101(10):3338–3345.
34. Onoyama I, et al. Conditional inactivation of Fbxw7 impairs cell-cycle exit during T cell differentiation and results in lymphomatogenesis. *J Exp Med.* 2007;204(12):2875–2888.
35. Matsuoka S, et al. Fbxw7 acts as a critical fail-safe against premature loss of hematopoietic stem cells and development of T-ALL. *Genes Dev.* 2008;22(8):986–991.
36. Ishikawa Y, Onoyama I, Nakayama KI, Nakayama K. Notch-dependent cell cycle arrest and apoptosis in mouse embryonic fibroblasts lacking Fbxw7. *Oncogene.* 2008;27(47):6164–6174.
37. Matteoni CA, Younossi ZM, Gramlich T, Boparai N, Liu YC, McCullough AJ. Nonalcoholic fatty liver disease: a spectrum of clinical and pathological

severity. *Gastroenterology.* 1999;116(6):1413–1419.
38. Horton JD, et al. Combined analysis of oligonucleotide microarray data from transgenic and knockout mice identifies direct SREBP target genes. *Proc Natl Acad Sci U S A.* 2003;100(21):12027–12032.
39. Kim BJ, Fulton AB. The genetics and ocular findings of Alagille syndrome. *Semin Ophthalmol.* 2007;22(4):205–210.
40. Loomes KM, et al. Bile duct proliferation in liver-specific Jag1 conditional knockout mice: effects of gene dosage. *Hepatology.* 2007;45(2):323–330.
41. Nishikawa Y, et al. Transdifferentiation of mature rat hepatocytes into bile duct-like cells in vitro. *Am J Pathol.* 2005;166(4):1077–1088.
42. McCright B, Lozier J, Gridley T. A mouse model of Alagille syndrome: Notch2 as a genetic modifier of Jag1 haploinsufficiency. *Development.* 2002;129(4):1075–1082.
43. McDaniell R, et al. NOTCH2 mutations cause Alagille syndrome, a heterogeneous disorder of the notch signaling pathway. *Am J Hum Genet.* 2006; 79(1):169–173.
44. Kodama Y, Hijikata M, Kageyama R, Shimotohno K, Chiba T. The role of notch signaling in the development of intrahepatic bile ducts. *Gastroenterology.* 2004;127(6):1775–1786.
45. Suzuki A, et al. Flow-cytometric separation and enrichment of hepatic progenitor cells in the developing mouse liver. *Hepatology.* 2000;32(6):1230–1239.
46. Leclercq IA, Farrell GC, Schriemer R, Robertson GR. Leptin is essential for the hepatic fibrogenic response to chronic liver injury. *J Hepatol.* 2002;37(2):206–213.
47. Sahai A, et al. Obese and diabetic *db/db* mice develop marked liver fibrosis in a model of nonalcoholic steatohepatitis: role of short-form leptin receptors and osteopontin. *Am J Physiol Gastrointest Liver Physiol.* 2004;287(5):G1035–G1043.
48. Horie Y, et al. Hepatocyte-specific Pten deficiency results in steatohepatitis and hepatocellular carcinomas. *J Clin Invest.* 2004;113(12):1774–1783.
49. Luedde T, et al. Deletion of NEMO/IKKgamma in liver parenchymal cells causes steatohepatitis and hepatocellular carcinoma. *Cancer Cell.* 2007; 11(2):119–132.
50. Isoda K, et al. Deficiency of interleukin-1 receptor antagonist deteriorates fatty liver and cholesterol metabolism in hypercholesterolemic mice. *J Biol Chem.* 2005;280(8):7002–7009.
51. Nakanishi Y, et al. Nonalcoholic steatohepatitis and hepatocellular carcinoma in galectin-3 knockout mice. *Hepatol Res.* 2008;38(12):1241–1251.
52. Yanagitani A, et al. Retinoic acid receptor alpha dominant negative form causes steatohepatitis and liver tumors in transgenic mice. *Hepatology.* 2004;40(2):366–375.
53. Nakayama H, et al. Transgenic mice expressing nuclear sterol regulatory element-binding protein 1c in adipose tissue exhibit liver histology similar to nonalcoholic steatohepatitis. *Metabolism.* 2007;56(4):470–475.
54. Consortium ECTS. Identification and characterization of the tuberous sclerosis gene on chromosome 16. *Cell.* 1993;75(7):1305–1315.
55. van Slegtenhorst M, et al. Identification of the tuberous sclerosis gene TSC1 on chromosome 9q34. *Science.* 1997;277(5327):805–808.
56. Li Z, White P, Tuteja G, Rubins N, Sackett S, Kaestner KH. Foxa1 and Foxa2 regulate bile duct development in mice. *J Clin Invest.* 2009;119(6):1537–1545.
57. Kuhn R, Schwenk F, Aguet M, Rajewsky K. Inducible gene targeting in mice. *Science.* 1995; 269(5229):1427–1429.
58. Postic C, Magnuson MA. DNA excision in liver by an albumin-Cre transgene occurs progressively with age. *Genesis.* 2000;26(2):149–150.
59. Tanigaki K, et al. Regulation of alphabeta/gammadelta T cell lineage commitment and peripheral T cell responses by Notch/RBP-J signaling. *Immunity.* 2004;20(5):611–622.
60. de Alboran IM, et al. Analysis of C-MYC function in normal cells via conditional gene-targeted mutation. *Immunity.* 2001;14(1):45–55.
61. Kamura T, et al. Cytoplasmic ubiquitin ligase KPC regulates proteolysis of $p27^{Kip1}$ at G1 phase. *Nat Cell Biol.* 2004;6(12):1229–1235.
62. Nishiyama M, Nakayama K, Tsunematsu R, Tsukiyama T, Kikuchi A, Nakayama KI. Early embryonic death in mice lacking the beta-catenin-binding protein Duplin. *Mol Cell Biol.* 2004;24(19):8386–8394.
63. Morita S, Kojima T, Kitamura T. Plat-E: an efficient and stable system for transient packaging of retroviruses. *Gene Ther.* 2000;7(12):1063–1066.